

# Emitting Electron Spectra and Acceleration Processes in the Jet of PKS 0447-439

Yao ZHOU, Dahai YAN, Benzhong DAI, and Li ZHANG  
*Department of physics, Yunnan University, Kunming, China*  
lizhang@ynu.edu.cn

(Received ; accepted )

## Abstract

We investigate the electron energy distributions (EEDs) and the corresponding acceleration processes in the jet of PKS 0447–439 and estimate its redshift through modeling its observed spectral energy distribution (SED) in the frame of a one-zone synchrotron-self Compton (SSC) model. Three EEDs formed in different acceleration scenarios are assumed: the power-law with exponential cut-off (PLC) EED (shock-acceleration scenario or the case of the EED approaching equilibrium in the stochastic-acceleration scenario), the log-parabolic (LP) EED (stochastic-acceleration scenario and the acceleration dominating) and the broken power law (BPL) EED (no acceleration scenario), and then the corresponding fluxes of both synchrotron and SSC are calculated. The model is applied to PKS 0447-439 and modeling SEDs are compared to the observed SED of this object by using the Markov Chain Monte Carlo (MCMC) method. Calculating results show that PLC model fails to fit the observed SED well, while the LP and BPL models give comparably good fits for the observed SED. The results indicate that it is possible that stochastic acceleration process acts in the emitting region of PKS 0447-439 and the EED is far from equilibrium (acceleration dominating) or no acceleration process works (in the emitting region). The redshift of PKS 0447-439 is also estimated in our fitting, and  $z = 0.16 \pm 0.05$  for LP case and  $z = 0.17 \pm 0.04$  for BPL case.

**Key words:** Acceleration of particles - Galaxies: BL Lacertae objects: individual (PKS 0447–439) - Galaxies: distances and redshifts - Gamma rays: theory

## 1. Introduction

PKS 0447-439, a high-frequency peaked BL Lac object (HBL), is one of the brightest source observed by the large Area Telescope (LAT) instrument on board of *Fermi* telescope. Motivated by the *Fermi*/LAT observation, the H.E.S.S. IACT observed PKS 0447-439 between November 2009 to January 2010 for 3.5 hours in total. During the H.E.S.S. campaign *Swift* observed PKS 0447-439 at optical-X-ray bands for about one week (Abramowski et al. 2013). Therefore, a high-quality multi-band SED has been built (Prandini et al. 2012; Abramowski et al. 2013). However, the redshift of PKS 0447-439 is not determined so far due to its weak emission lines. Its redshift has been measured by many authors with different method. Craig et al. (1997) gave the estimate of the redshift with  $z = 0.107$ . Perlman et al. (1998) reported a value of  $z = 0.205$  based on a very weak spectral feature, which were interpreted as the Ca line with doubt lately. Landt & Bignall (2008) gave a lower limit of 0.176. Recently, Landt et al. (2012) put a high lower limit of  $z > 1.246$  based on the weak absorption lines which however was defined as atmospheric absorption lines by the detection of Pita et al. (2012). On the other hand, the redshift of PKS 0447-439 can be estimated through combining its observed GeV-TeV spectrum, for example, Prandini et al. (2012) suggested that its redshift is likely 0.2, and Abramowski et al. (2013) pointed out that the most conservative upper limit of this

object is  $z < 0.59$ .

It is well known that the multi-band emission from a blazar with synchrotron peak in UV-X-ray bands (HBL) can be explained in the frame of a one-zone SSC model (e.g., Tavecchio et al. (1998); Finke et al. (2008); Zhang et al. (2012)). In this model, the spectral energy distribution (SED) for a blazar consists of two bumps, the first bump can be explained by synchrotron emission of relativistic electrons, and the second bump could be produced by relativistic electrons inverse Compton (IC) scattering with photons which come from synchrotron emission (synchrotron self-Compton, SSC; e.g., Rees (1967); Maraschi et al. (1992)). Note that besides the classic one-zone model, a kind of two-zone (acceleration zone and cooling zone) model has been proposed (e.g., Kirk et al. (1998); Kusunose et al. (2000); Fan et al. (2008); Weidinger et al. (2010); Weidinger & Spanier (2010)). Here we will focus on the one-zone SSC model.

In modeling SED of a blazar in the one-zone SSC model, an important physics quantity is the emitting electron distribution (EED). The form of EED can give information about acceleration and cooling processes. Generally, there are three kinds of EEDs formed in different scenarios. The first one is the power-law with exponential cut-off (PLC) EED which is usually believed to be formed in the Fermi I acceleration process (shock acceleration) (e.g., Drury et al. (1994); Kirk et al. (1998); Kusunose et al. (2000)). However, recent studies indicate that the PLC can be obtained also in a scenario where Fermi II

(or both Fermi I and Fermi II) acceleration processes act in the case of EED approaching the equilibrium (e.g., Weidinger et al. (2010); Tramacere et al. (2011); Yan et al. (2012)). The second one is the log-parabolic (LP) EED which can be formed in the Fermi II acceleration process (stochastic acceleration) in the case of the acceleration process dominating over the radiative cooling (e.g., Becker et al. (2006); Tramacere et al. (2011)). The third one is that no acceleration process is considered in the emitting region, the injected EED can indicate the acceleration process (e.g., Chiaberge & Ghisellini (1999); Kataoka et al. (2000); Li & Kusunose (2000); Böttcher & Chiang (2002); Chen et al. (2011); Chen et al. (2012)) and the EED can be approximated by a broken power law (BPL) (e.g., Dermer & Menon 2009; Böttcher et al. 2013; Finke 2013). Many authors have studied the emission mechanisms in the three scenarios by using time-dependent models (e.g., Böttcher & Chiang 2002; Tramacere et al. 2011; Zheng et al. 2011; Yan et al. 2012). For simplicity we use static EEDs here. In a simplified one-zone SSC model, the EEDs and acceleration processes in the jet of HBL can be investigated through modeling the high-quality SED (e.g. Yan et al. 2013).

In this work, after assuming three EEDs formed in the three scenarios described above we investigate the EEDs and acceleration processes in the jet of PKS 0447-439 through fitting its quasi-simultaneous SED with a simplified one-zone SSC model. In order to obtain more efficient constraints on the model parameters, we employ MCMC method to investigate the high-dimensional model parameter spaces systematically. The redshift of PKS 0447-439 is also estimated in the fitting. We adopt the cosmological parameters  $(H_0, \Omega_m, \Omega_\Lambda) = (70 \text{ km s}^{-1} \text{ Mpc}^{-1}, 0.3, 0.7)$  throughout this paper.

## 2. Modelling SED

We will model the SED in the frame of a one-zone SSC model given by Finke et al. (2008). In this model, the non-thermal multi-wavelength emission is assumed to be produced by both the synchrotron radiation and SSC process of relativistic electrons in a homogeneous blob of the jet, which is moving relativistically at a small angle to our line of sight, and the observed radiation is strongly boosted by a relativistic Doppler factor. There are three model parameter characterizing the global properties of the blob: the magnetic field intensity in the emitting blob  $B$ , the Doppler factor  $\delta_D$  and the radius of the blob  $R'_b = t_{v,\min} \delta_D c / (1+z)$  where  $t_{v,\min}$  is the minimum variability timescale in the observer's frame. Here, quantities in the observer's frame are unprimed, and quantities in the comoving frame are primed. Note that the magnetic field  $B$  is defined in the comoving frame, despite being unprimed.

### 2.1. Emitting Electron Distributions

For the relativistic electrons distribution in the blob, three cases we described in Introduction are considered. If there exists acceleration process in the emitting blob,

two forms of EEDs (PLC and LP) could be generated. The PLC electron distribution is

$$N'(\gamma') \sim \left(\frac{\gamma'}{\gamma'_c}\right)^{-s} \exp\left(\frac{-\gamma'}{\gamma'_c}\right) \text{ for } \gamma'_{\min} \leq \gamma' \leq \gamma'_{\max}, \quad (1)$$

where  $s$  is the electron energy spectral index, and  $\gamma'_c$  is the high energy cut-off. The LP EED generated in the framework of stochastic-turbulence-acceleration is

$$N'(\gamma') \sim \begin{cases} \left(\frac{\gamma'}{\gamma'_c}\right)^{-s} & \gamma'_{\min} \leq \gamma' \leq \gamma'_c \\ \left(\frac{\gamma'}{\gamma'_c}\right)^{-[s+r \log(\frac{\gamma'}{\gamma'_c})]} & \gamma'_c \leq \gamma' \leq \gamma'_{\max}, \end{cases} \quad (2)$$

where  $r$  is the curvature term of EED (Massaro et al. 2006). In the above two cases,  $\gamma'_c$  is determined by the competition between acceleration process and energy losses of electrons. The spectral index  $s$  is controlled by the acceleration and escape timescales  $t_{\text{acc}}$  and  $t_{\text{esc}}$  or the duration of the injection (impulsive or continuous) (e.g. Katarzyński et al. 2006).

If there is no acceleration process in the emitting blob, the cooled EED in the blob is the BPL shape. Here, we use the BPL electrons distribution given by Dermer et al. (2009), i.e.,

$$N'_e(\gamma') \sim H(\gamma'; \gamma'_{\min}, \gamma'_{\max}) \{ \gamma'^{-p_1} \exp(-\gamma'/\gamma'_b) \\ \times H[(p_2 - p_1)\gamma'_b - \gamma'] + [(p_2 - p_1)\gamma'_b]^{p_2 - p_1} \gamma'^{-p_2} \\ \times \exp(p_1 - p_2) H[\gamma' - (p_2 - p_1)\gamma'_b] \}, \quad (3)$$

where  $H(x; x_1, x_2)$  is the Heaviside function:  $H(x; x_1, x_2) = 1$  for  $x_1 \leq x \leq x_2$  and  $H(x; x_1, x_2) = 0$  everywhere else; as well as  $H(x) = 0$  for  $x < 0$  and  $H(x) = 1$  for  $x \geq 0$ .  $\gamma'_{\min}$  and  $\gamma'_{\max}$  are the minimum and maximum energies of electrons, respectively.  $p_1$  and  $p_2$  are the spectral indices below and above the electron's break energy  $\gamma'_b$ . In this case,  $\gamma'_b$  is determined by the energy losses and escape of electrons. The injection process (i.e., the injected spectrum and the injection time) and evolution time determines  $p_1$  and  $p_2$ . Note that only when  $\gamma'_c$  of the injected EED  $\gg \gamma'_b$  which means significant energy losses, the cooled EED can be the BLP shape distinctly. In all of the three cases, we use the factor  $U'_e/U'_B$  to normalize the electrons numbers in the emitting blob.

### 2.2. Synchrotron and SSC Fluxes

The synchrotron flux and the SSC flux are calculated as in Finke et al. (2008). The synchrotron flux is

$$\nu F_\nu^{\text{syn}} = \frac{\sqrt{3} \delta_D^4 \epsilon' e^3 B'}{4 \pi h d_L^2} \int_0^\infty d\gamma' N'_e(\gamma') (4 \pi R_b'^3 / 3) R(x), \quad (4)$$

where  $e$  is the electron charge,  $B'$  is the magnetic field strength,  $R'_b$  is blob's radius,  $h$  is the Planck constant, and  $d_L$  is the distance to the source with a redshift  $z$ . Here  $m_e c^2 \epsilon' = h \nu (1+z) / \delta_D$  is synchrotron photons energy in the co-moving frame, where  $m_e$  is the rest mass of electron and  $c$  is the speed of light. Here we use an approximation for  $R(x)$  given by Finke et al. (2008). The synchrotron spectral energy density is

$$u'_{\text{syn}}(\epsilon') = \frac{R'_b}{c} \frac{\sqrt{3} e^3 B'}{h} \int_0^\infty d\gamma' N'_e(\gamma') R(x). \quad (5)$$

The SSC flux is

$$\nu F_{\nu}^{\text{SSC}} = \frac{3}{4} c \sigma_T \epsilon_s'^2 \frac{\delta_D^4}{4\pi d_L^2} \int_0^\infty d\epsilon' \frac{u'_{\text{syn}}(\epsilon')}{\epsilon'^2} \times \int_{\gamma'_{\min}}^{\gamma'_{\max}} d\gamma' \frac{N'_e(\gamma')(4\pi R_b'^3/3)}{\gamma'^2} F_C(q', \Gamma'_e), \quad (6)$$

where  $\sigma_T$  is the Thomson cross section,  $m_e c^2 \epsilon'_s = h\nu(1+z)/\delta_D$  is the energy of IC scattered photons in the co-moving frame,  $F_C(q', \Gamma'_e) = 2q' \ln q' + (1+2q')(1-q') + \frac{q'^2 \Gamma_e'^2}{2(1+q' \Gamma_e')} (1-q')$ ,  $q' = \frac{\epsilon'/\gamma'}{\Gamma_e'(1-\epsilon'/\gamma')}$ ,  $\Gamma_e' = 4\epsilon' \gamma'$ , and  $\frac{1}{4\gamma'^2} \leq q' \leq 1$ .

Very high energy (VHE) photons emitted by blazars are effectively absorbed through the pair-production process, by the interaction with extragalactic background light (EBL) (e.g., Stecker et al. 1992). The absorption effect depends on both the EBL photon density and the redshift of the TeV source. EBL is mainly composed of stellar light and the reprocessed emission produced by stellar dust. Due to the bright foreground (e.g., the zodiacal light and the stellar light from Milky Way), direct measurements of the EBL become very difficult. Then, many EBL models are proposed, such as Inoue et al. (2013); Gilmore et al. (2012); Domínguez et al. (2011); Kneiske & Dole (2010); Finke et al. (2010); Razzaque et al. (2009); Franceschini et al. (2008); Stecker et al. (2006). In this work we use the EBL model of Finke et al. (2010) which is believed to be correct in high confidence level (Ackermann et al. 2012), to correct the EBL absorption.

### 2.3. Fitting Method

Because the MCMC method which is based on Bayesian statistics is more efficient for sampling of the parameter spaces, it has been frequently used to fit the SEDs of blazars and supernova remnants (SNRs) in order to investigate high-dimensional parameter spaces (e.g., Yuan et al. 2011; Yan et al. 2013). In this MCMC method the Metropolis-Hastings sampling algorithm, which ensures that the probability density functions of model parameters can be asymptotically approached with the number density of samples, is adopted to determine the jump probability from one point to the next in parameter space (Mackay et al. 2003). Neal et al. (1993); Gamerman et al. (1997); Mackay et al. (2003) have given more details about the MCMC method. In this work, we assumed flat priors in the model parameter spaces and run single chains using the Raftery et al. (1992) convergence diagnostics. The MCMC code we used in this work (Liu et al. 2012) is adapted from COSMOMC (Lewis et al. 2002). Hence, more information of the COSMOMC code about the sampling options, convergence criteria, and statistical quantities can be found in the website<sup>1</sup> and Lewis et al. (2002) and references therein.

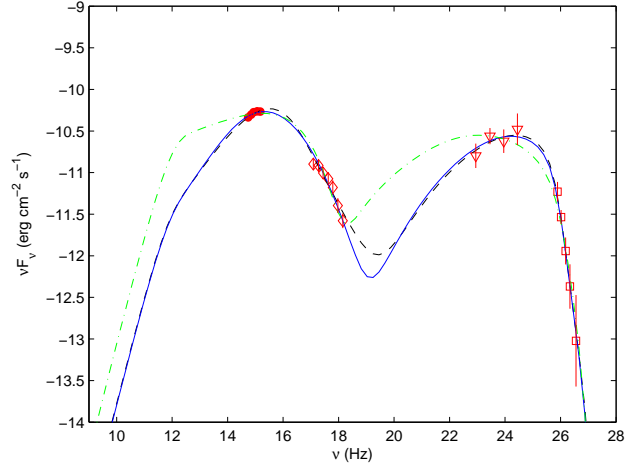


**Fig. 1.** SED of PKS 0447-439. The quasi-simultaneous data are *Swift*/UVOT (circle), *Swift*/XRT (diamond), *Fermi*/LAT (triangle) and H.E.S.S. (square) data. The lines are the results of SSC model for three EEDs: BPL (dashed line), LP (solid line) and PLC (dash-dotted line).

### 3. The results

In this work, we adopt the quasi-simultaneous SED of PKS 0447-439 reported in Prandini et al. (2012), which includes the *Swift*/UVOT, *Swift*/XRT, *Fermi*/LAT and H.E.S.S. data observed during November 2009 - January 2010. In our fittings, we fix  $\gamma'_{\min} = 400$  and  $\gamma'_{\max} = 10^8$  for the three cases. Meanwhile, we use  $t_{v,\min} = 1$  day as its upper limit because of a signature of variability at X-ray energies on timescale of one day (Prandini et al. 2012). We also set an upper limit for Doppler factor,  $\delta_D \leq 50$  to avoid the extreme value. In our fittings the redshift is taken as a free parameter since the redshift of a HBL can be constrained through fitting its SED including the GeV and TeV data (e.g., Acciari et al. 2010; Abdo et al. 2011; Yan et al. 2013; Abramowski et al. 2013). In this method of estimating the redshift, the intrinsic VHE spectrum is obtained by fitting the observed SED covering from optical to GeV energies. Through comparing the EBL corrected intrinsic VHE spectrum (depending on the redshift) and the observed VHE spectrum, the redshift can be inferred (Acciari et al. 2010; Yan et al. 2013).

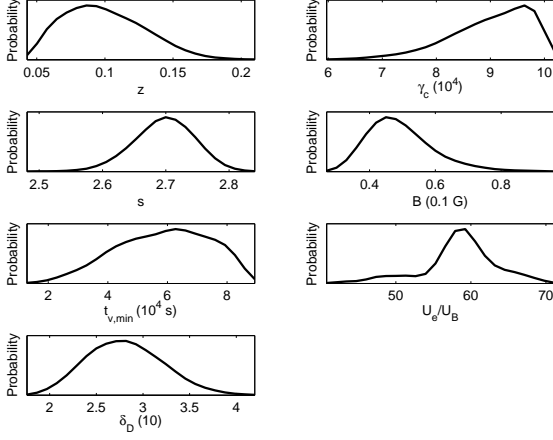
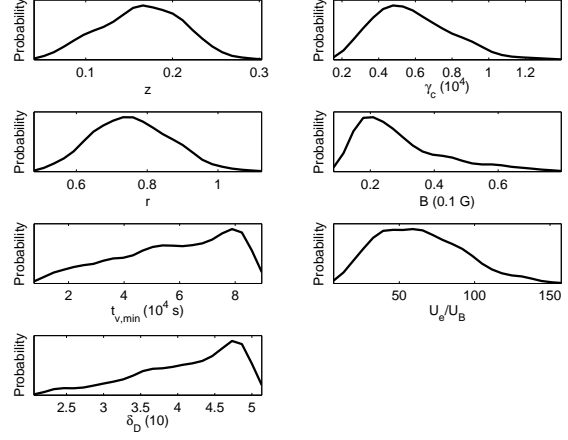
The SED modeling results are shown in Fig. 1. The marginalized best-fit parameter values and their 68% confidence limits are summarized in Table 1. The marginalized one-dimensional (1D) probability distributions of the model parameters are shown in Fig. 2 (the PLC case), Fig. 3 (the LP case), and Fig. 4 (the BPL case).

For the PLC case, there are seven parameters, which are  $B$ ,  $\delta_D$ ,  $t_{v,\min}$ ,  $s$ ,  $\gamma'_c$ ,  $U'_e/U'_B$ , and  $z$  (Table 1). It can be found the fitting at GeV bands is bad (dash-dotted line in Fig. 1 and  $\chi^2_\nu$  in Table 1). The cutoff energy  $\gamma'_c$  is poorly constrained. Therefore, the redshift obtained in this case is incredible.

<sup>1</sup> <http://cosmologist.info/cosmomc/>

**Table 1.** The marginalized best-fit model parameters, their 68% confidence limits and the reduced  $\chi^2_\nu$  values for three EEDs.

Model	$z$	$\gamma'_c, \gamma'_b$ ( $10^4$ )	$s, r, p_2$	$B$ (0.1 G)	$t_{v,\min}$ ( $10^4$ s)	$\delta_D$ (10)	$U'_e/U'_B$	$\chi^2_\nu$
PLC model	0.10	8.99	2.70	0.50	5.86	2.81	58.45	1.48
68% limit	(0.09-0.13)	(8.24-10.00)	(2.65-2.74)	(0.40-0.59)	(4.19-7.53)	(2.40-5.0)	(55.11-62.56)	-
LP model	0.16	0.59	0.76	0.29	5.79	4.11	63.83	0.49
68% limit	(0.11-0.21)	(0.38-0.81)	(0.65-0.87)	(0.17-0.44)	(3.46-8.60)	(3.37-5.0)	(34.73-93.58)	-
BPL model	0.17	3.33	4.26	0.30	5.42	4.22	61.09	0.45
68% limit	(0.13-0.21)	(2.70-3.91)	(4.10-4.42)	(0.18-0.43)	(2.86-8.60)	(3.58-5.0)	(35.02-85.89)	-

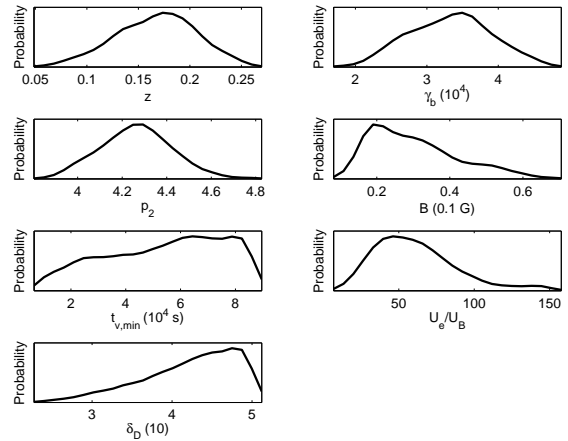
**Fig. 2.** 1D marginalized probability distribution of the parameters for PLC EED.**Fig. 3.** 1D marginalized probability distribution of the parameters for LP EED.

For the LP case, since we fix the electron energy index  $s = 2.0$  according to the result of Prandini et al. (2012), there are also seven parameters, which are  $B$ ,  $\delta_D$ ,  $t_{v,\min}$ ,  $r$ ,  $\gamma'_c$ ,  $U'_e/U'_B$  and  $z$  (see Table 1). It can be seen that the fitting in this case becomes good (solid line in Fig. 1). The parameters describing the EED:  $\gamma'_c$ ,  $r$  and  $U_e/U_B$  are all constrained well. However, the constraints on  $\delta_D$  and  $t_{v,\min}$  are poor, and both parameters tend to be larger than the upper limits we set. In this case, the redshift is constrained well with  $z = 0.16 \pm 0.05$ .

For the BPL case, we also fix  $p_1 = 2.0$  and there are also seven parameters, which are  $B$ ,  $\delta_D$ ,  $t_{v,\min}$ ,  $p_2$ ,  $\gamma'_b$ ,  $U_e/U_B$  and  $z$  (see Table 1). In this case, the fitting (dashed line in Fig. 1) is comparably good compared with that in the LP case. The constraints on the parameters are almost the same as those in the LP case. In this case, the redshift is also constrained well with  $z = 0.17 \pm 0.04$ .

#### 4. DISCUSSION AND CONCLUSIONS

Using the MCMC method, we fitted the SED of PKS 0447-439 in the one-zone SSC model for three kinds of EEDs having clear physical meanings: PCL, LP and BPL EEDs. Our results show that the SED of PKS 0447-439 can be fitted well for LP and BPL EEDs. As mentioned in §1, the LP shape EED can be formed in the stochastic acceleration process when the acceleration timescale

**Fig. 4.** 1D marginalized probability distribution of the parameters for BPL EED.



is shorter than the cooling timescale. The BPL shape EED can be formed in the emitting blob where no acceleration process works, and the broken energy  $\gamma'_b$  is determined when the cooling timescale is equal to the escape timescale. Our results indicate that the multi-band emissions of PKS 0447-439 originate in a blob where either the stochastic acceleration dominates over the cooling or no acceleration process works. It can be inferred in Fig. 1 (according to the peak fluxes of synchrotron and SSC components) that the synchrotron cooling is comparable to the SSC cooling. The synchrotron time is  $t_{\text{syn}}^{\text{cool}} \approx 7.8 \times 10^8 / (\gamma' B^2)$ . In the LP case, taking  $\gamma' = \gamma'_c$ , we obtain  $t_{\text{syn}}^{\text{cool}} \approx 1.6 \times 10^8$  s. Hence, in the stochastic acceleration case the acceleration timescale should be less than  $\sim 10^8$  s. The inefficient coolings is attributed to the small magnetic field strength and then the low synchrotron photon density, and in this case the relatively large size of blob is required ( $R'_b \approx 7.2 \times 10^{16}$  cm). It is hard to distinguish LP EED from BPL EED based on the current observations. In Fig. 1, however, we note that the case of BPL predicts higher  $\nu F_\nu$  fluxes at  $\sim 20$ -50 keV than the fluxes predicted in the case of LP. Therefore, the observations of The Nuclear Spectroscopic Telescope Array (NuSTAR) (Harrison et al. 2013) at 6-80 keV may be helpful to distinguish BLP scenario from LP scenario. The alternative way to distinguish BLP scenario from LP scenario may be the observed minimum variability timescale  $t_{v,\text{min}}$  since our fitting results show that  $t_{v,\text{min}} > 2.86 \times 10^4$  s for BLP EED while  $t_{v,\text{min}} > 3.46 \times 10^4$  s for LP EED. Our results can be used as a preliminary indicator for the detailed studies of the acceleration processes in the jet to simplify the physical model and reduce the model parameters.

Due to the weak emission line of the HBL, the classical spectrographic measurement of redshift is invalid sometimes. Thanks to the observations at GeV and TeV bands, an alternative method to estimate the redshift of HBL is to fit its GeV-TeV spectra with the certain emission model (e.g., Acciari et al. 2010; Abdo et al. 2011; Yan et al. 2013). With more powerful MCMC method, our results show that in the frame of one-zone SSC model, the redshift of PKS 0447-439 is between 0.11 and 0.21 and the most likely redshift is 0.16 and 0.17 which are basically consistent with the results estimated by other authors with different methods (e.g., Prandini et al. 2012; Abramowski et al. 2013; Perlman et al. 1998; Landt & Bignall 2008). There is no discrepancy between the redshift derived in the LP case and BPL case. Our results depend on the EBL model. The recent believable study indicated that the real EBL intensity may be slightly weaker than the prediction by the EBL model of Finke et al. (2010), which should be scaled by the factor  $0.86 \pm 0.23$  (Ackermann et al. 2012). We found that when the EBL model of Finke et al. (2010) is scaled by the factor 0.86, the estimate on the redshift is not changed.

We note that the jet of PKS 0447-439 appears to be particle dominated ( $U'_e/U'_B \approx 60$ ; see Table 1). It seems that the jets of the HBLs (e.g., Mrk 421 and Mrk 501) whose high energy emissions can be explained with one compo-

nent tends to be particle dominated (e.g., Mankuzhiyil et al. 2012; Yan et al. 2013; Zhang et al. 2013), while the jets of flat spectrum radio quasars (FSRQs; e.g., 3C 279) whose high energy emissions require multi-component origination could tend to achieve equipartition between the energies of emitting electrons and magnetic field (e.g., Dermer et al. (2013); Zhang et al. (2013)). More considerations are needed on this issue.

## Acknowledgments

We thank the anonymous referee for his/her very constructive suggestions. We acknowledge the support of Yunnan University's Science Foundation for graduate student under grant No. YNUY201260 and the Science Foundation for graduate student of Provincial Education Department of Yunnan under grant No. 2013J071. This work is partially supported by the 973 Programme (2009CB824800). B.Z.D. acknowledges the support of National Natural Science Foundation of China under grants No. 11063003.

## References

- Abdo, A. A., et al. (Fermi-LAT collaboration), 2011, *ApJ*, 726, 43
- Abramowski A., et al.(H.E.S.S. Collaboration), 2013, *A&A*, 552A, 118
- Ackermann, M., Ajello, M., Allafort, A. et al., 2012, *Sci*, 338, 1190
- Acciari V. A. et al., 2010, *ApJ*, 708, 100
- Becker, P. A., Le, T., & Dermer, C. D. 2006, *ApJ*, 647, 53
- Böttcher, M., & Chiang, J. 2002, *ApJ*, 581, 127
- Böttcher, M., Reimer, A., Sweeney, K., Prakash, A. 2013, *ApJ*, 768, 54
- Chen, X., Fossati, G., Liang, E. P., Böttcher, M. 2011, *MNRAS*, 416, 2368
- Chen, X., Fossati, G., Böttcher, M., Liang, E. P. 2012, *MNRAS*, 424, 789
- Chiaberge, M. & Ghisellini, G., 1999, *MNRAS*, 306, 551
- Craig, N. & Fruscione, A., 1997, *Astron. J.* 114, 1356
- Dermer, C. D. & Menon, G. 2009, *High Energy Radiation from Black Holes: Gamma Rays, Cosmic Rays, and Neutrinos* (Princeton University Press)
- Dermer C. D., Finke J. D., Krug H., 2009, *ApJ*, 692, 32 43
- Dermer, C. D., Cerruti, M., Lott, B., Boisson, C., Zech, A., 2013, arXiv: 1304.6680
- Domínguez, A., Primack, J. R., Rosario, D. J. et al., 2011, *MNRAS*, 410, 2556
- Drury, L., Aharonian, F., & Völk, H. 1994, *A&A*, 287, 959
- Fan, Z. H., Liu, S. M., Wang, J. M., Fryer, C. L., Li, H., 2008, *ApJ*, 673, 139
- Finke J. D., Dermer C. D., Böttcher M., 2008, *ApJ*, 686, 181
- Finke, J. D., Razzaque, S., & Dermer, C. D. 2010, *ApJ*, 712, 238
- Finke J. D., 2013, *ApJ*, 763, 134
- Franceschini, A., Rodighiero, G., & Vaccari, M. 2008, *A&A*, 487, 837
- Li, H., & Kusunose, M. 2000, *ApJ*, 536, 729

- Gamerman, D. 1997, *Markov Chain Monte Carlo: Stochastic Simulation for Bayesian Inference* (London: Chapman and Hall)
- Gilmore R. C., Somerville R. S., Primack J. R., Domínguez, A., 2012, *MNRAS*, 422, 3189
- Harrison, F. A., Craig, W. W., Christensen, F. E. et al. 2013, *ApJ*, 770, 103
- Inoue Y., Inoue S. Kobayashi M., Makiya R. Niino Y. Totani, T., 2013, *ApJ*, 768, 197
- Kataoka, J., Takahashi, T., Makino, F., Inoue, S., Madejski, G. M., Tashiro, M., Urry, C. M., Kubo, H. 2000, *ApJ*, 528, 243
- Katarzyński, K., Ghisellini, G., Mastichiadis, A., Tavecchio, F., Maraschi, L. 2006, *A&A*, 453, 47
- Kirk, J. G., Rieger, F. M., & Mastichiadis, A. 1998, *A&A*, 333, 452
- Kneiske, T. M., & Dole, H. 2010, *A&A*, 515, A19
- Kusunose M., Takahara F., & Li, H., 2000, *ApJ*, 536, 299
- Landt, H., 2012, *MNRAS Lett.*, 423, 84
- Landt, H. & Bignall, H. E., 2008, *MNRAS*, 391, 967
- Lewis, A., & Bridle, S. 2002, *PhRvD*, 66, 103511
- Liu, J., Yuan, Q., Bi, X. J., Li, H., & Zhang, X. M. 2012, *PhRvD*, 85, 3507
- Mackay, D. J. C. 2003, *Information Theory, Inference and Learning Algorithms* (Cambridge: Cambridge Univ. Press)
- Maraschi, L., Ghisellini, G., & Celotti, A. 1992, *ApJL*, 397, L5
- Mankuzhiyil, N., Ansoldi, S., Persic, M., Rivers, E., 2012, *ApJ*, 753, 154
- Massaro, E., Tramacere, A., Perri, M., Giommi, P., Tosti, G. 2006, *A&A*, 448, 861
- Neal, R. M. 1993, *Probabilistic Inference Using Markov Chain Monte Carlo Methods* (Canada: Department of Computer Science, Univ. Toronto)
- Perlman, E. S. et al., 1998, *ApJ*, 115, 1253
- Pita, S., Goldoni, P., Boisson, C. et al. 2012, proceedings of the Gamma 2012 conference, astro-ph/1208.1785
- Prandini, E. et al., 2012, *A&A* 543A, 111
- Raftery, A. E., & Lewis, S. M. 1992, *StaSc*, 7, 493
- Razzaque, S., Dermer, C. D., & Finke, J. D. 2009, *ApJ*, 697, 483
- Rees, M. J. 1967, *MNRAS*, 137, 429
- Stecker, F. W., de Jager, O. C., & Salamon, M. H. 1992, *ApJ*, 390, L49
- Stecker, F. W., Malkan, M. A., & Scully, S. T. 2006, *ApJ*, 648, 774
- Tavecchio, F., Maraschi, L., Ghisellini, G., 1998, *ApJ*, 509, 608
- Tramacere, A., Massaro, E., & Taylor, A. M. 2011, *ApJ*, 739, 66
- Weidinger M., Rüger M., Spanier F., 2010, *Astrophys. Space Sci. Trans.*, 6, 1
- Weidinger M., & Spanier F., 2010, *A&A*, 515, 18
- Yan, D. H., Fan Z. H., Zhou, Y., Dai B. Z. 2013, *RAA*, 13,411
- Yan, D. H., Zhang L., Yuan, Q., Fan, Z. H., Zeng, H. D., 2013, *ApJ*, 765,122
- Yan, D. H., Zeng, H. D., Zhang, L., 2012, *MNRAS*, 424,2173
- Yuan, Q., Liu, S. M., Fan, Z. H., Bi, X. J., Fryer, C. L., 2011, *ApJ*, 735, 120
- Zhang J., Liang E. W., Zhang S. N., Bai J. M. 2012, *ApJ*, 752, 157
- Zhang J., Sun X., Liang E. W., et al. 2013, arXiv:1307.6911
- Zheng Y. G., & Zhang L., 2011, *ApJ*, 728, 105